frontiers | Frontiers in Energy Research

TYPE Original Research
PUBLISHED 07 June 2024
DOI 10.3389/fenrg.2024.1363363



OPEN ACCESS

EDITED BY
Zequn Yang,
Central South University, China

REVIEWED BY
Junwei Yang,
City University of Hong Kong, Hong Kong SAR, China
Bo Jiang,
Nanjing University of Science and Technology, China
Feng Xin,
Changsha University of Science and Technology, China

*CORRESPONDENCE
Qinghai Chen,
zhangyindihust@foxmail.com

RECEIVED 30 December 2023
ACCEPTED 15 April 2024
PUBLISHED 07 June 2024

CITATION
Zhang Y, Xue Y, Xu Z, Zeng F, Xin Y, Chen Q and Takyi SA (2024), Effect of $H_2$/CO addition on soot formation in ethylene diffusion flame. *Front. Energy Res.* 12:1363363. doi: 10.3389/fenrg.2024.1363363



# Effect of $H_2$/CO addition on soot formation in ethylene diffusion flame

Yindi Zhang[1,2], Yijing Xue[1], Zichun Xu[3], Fanjin Zeng[1], Yue Xin[1], Qinghai Chen[4]* and Shadrack Adjei Takyi[1]

[1]School of Petroleum Engineering, Yangtze University, Wuhan, Hubei, China, [2]State Key Laboratory of Low Carbon Catalysis and Carbon Dioxide Utilization, Lanzhou Institute of Chemical Physics, Chinese Academy of Sciences, Lanzhou, Gansu, China, [3]Wuhan New Waterway—Wuhan Design and Engineering College A-Level Center, Wuhan, Hubei, China, [4]School of Urban Construction, Yangtze University, Jingzhou, Hubei, China

Coupling the San Diego gas phase reaction mechanism and the Moss Brookes soot model using FLUENT14.0 software, the effect of adding $H_2$/CO on the fuel side on soot formation in an ethylene/air laminar diffusion flame was studied. A specific analysis was conducted on the effects of $H_2$, CO and its chemical effects on flame temperature, soot volume fraction, mole fractions of important intermediate products OH, H, and $C_2H_2$, as well as rate of soot mass nucleation, surface growth, and oxidation. In the numerical calculation, the virtual substances $FH_2$ and FCO are set to separate the chemical effect of $H_2$ and CO and to analyze the chemical effect of adding $H_2$ and CO on soot formation. The results show that the flame temperature increases slightly, and the soot volume fraction decreases monotonically with adding $H_2$ and CO. The chemical effect of $H_2$ increases the temperature, the mole fraction of $C_2H_2$ and H, the soot nucleation rate, and the surface growth rate, and finally, it promotes soot formation. The chemical effect of CO increases the temperature and H mole fraction, reduces the OH mole fraction, and then increases the soot surface growth rate and reduces the soot oxidation rate. The higher soot nucleation, surface growth rate, and lower oxidation rate jointly promote soot formation.

KEYWORDS

**diffusion flame, $H_2$/CO addition, soot, chemical effect, numerical simulation**

## 1 Introduction

Fossil fuels still account for a large proportion of the current energy structure (Zeng et al., 2021; Li et al., 2022), and soot particles and $CO_2$ emissions results in greenhouse effect and human health. Soot is one of the primary pollutants generated during the incomplete combustion of fossil fuels, which will cause serious harm to the environment and human health (Shiraiwa et al., 2012; Sahu et al., 2016; Cocean et al., 2020). Therefore, the research on clean alternative fuels and renewable energy has received extensive attention. Syngas is a mixture of $H_2$ and CO mixed in different proportions. Gases usually contain some $CO_2$ and $CH_4$. Syngas is one of product of coal gasification which widely used in power plants and internal combustion engines. It can be used as alternative fuels to blend hydrocarbon fuels, improve combustion efficiency and reduce pollutant emissions (Mahgoub et al., 2017; Lapalme et al., 2018; Krishnamoorthi et al., 2020). CO, is an intermediate pollution produced by the combustion of carbon containing fuels, which emission control cannot be ignored for $CO_2$ reduction emission.

Some studies have shown the effect of blending $H_2$ and CO with hydrocarbon fuels on soot formation. Wang et al. (Wang K. et al., 2021) have performed a detailed numerical calculation of the combustion of natural gas with $H_2$ addition. The results show that with the increase in the $H_2$ blending ratio, the combustion rate accelerates, the temperature increases, and the soot and CO emissions decrease. Zhao et al., 2014 studied the effect of adding hydrogen and helium on soot formation in ethylene laminar diffusion flame through experiments. The results showed that adding hydrogen increased the flame temperature. Due to the dilution and direct chemical effect, adding hydrogen is more effective than helium in reducing soot formation. (Sun et al., 2017; Yen et al., 2019) studied the effect of blending $H_2$ and $N_2$ into ethylene/air diffusion flame on flame temperature and soot generation through experiments. The results showed that blending $H_2$ or $N_2$ significantly reduced soot volume fraction and primary particle size but had little effect on flame peak temperature. Wang et al., 2018 studied the effect of adding $H_2$ on soot formation in ethylene laminar diffusion flame in the $O_2/CO_2$ atmosphere through numerical simulation. The results showed that adding $H_2$ inhibited soot formation through dilution and chemical effect, and the chemical effect of $H_2$ reduced soot nucleation and oxidation rate. Wang et al. (Wang Y. et al., 2021) studied the effect of $H_2$ addition in methane and ethylene flames on the formation path of benzene. The numerical results show that adding hydrogen to ethylene diffusion flame decreases the soot nucleation and surface growth rate. Qiu et al., 2020 have numerically calculated the flame and soot formation characteristics of adding $H_2$ to the coflow laminar diffusion of ethylene. The results show that the soot is reduced after adding $H_2$. The various effects of $H_2$ addition were separated by adding multiple virtual substances in the gas phase mechanism, and it was found that the chemical effect of $H_2$ promotes soot formation. Kalbhor and Oijen, 2020 studied the effect of adding $H_2$ to fuel and $H_2O$ to oxidant on soot formation in laminar flow counter ethylene diffusion flame through numerical simulation. The results show that $H_2$ on the fuel side and $H_2O$ on the oxidant side inhibit soot formation through a chemical effect. Dai et al., 2020 studied the effect of adding CO to the counter-diffusion flame of ethylene and propane on the soot formation. They found that adding CO reduces the soot formation in the ethylene flame. The chemical effect of CO was separated from the dilution effect by adding $N_2$. The results show that the chemical effect of CO promotes soot formation. Jiang and Qiu, 2010 have performed a numerical calculation on adding CO to acetylene-premixed flames. The results show that the addition of CO gradually reduced the soot formation. The analysis of numerical results shows that adding CO reduces the concentration of OH radicals and thus slows down the oxidation rate of the soot and reduces acetylene concentration.

The current research shows that adding $H_2$ or CO to hydrocarbon fuel can inhibit soot formation in flames. Still, there is no unified conclusion about the inhibition mechanism of $H_2$ and CO, especially the effects of chemical effects on soot formation. This paper used CFD to perform a numerical simulation on blending $H_2$, and CO on the fuel side in a laminar coflow ethylene/air diffusion flame, and the effects of different $H_2$/CO blending ratios on ethylene flame temperature and soot formation were analyzed. The virtual substances $FH_2$ and FCO were constructed in the numerical calculation to separate the chemical effect of $H_2$ and CO. This study compares the changes in the mole fractions of important intermediate components and analyzed their effects on the rate of soot mass nucleation, surface growth, and oxidation.The mole fraction changes of important intermediate components were compared to study the effect of $H_2$/CO addition on soot formation and provide a reference for the soot emission reduction performance of syngas added to hydrocarbon fuel.

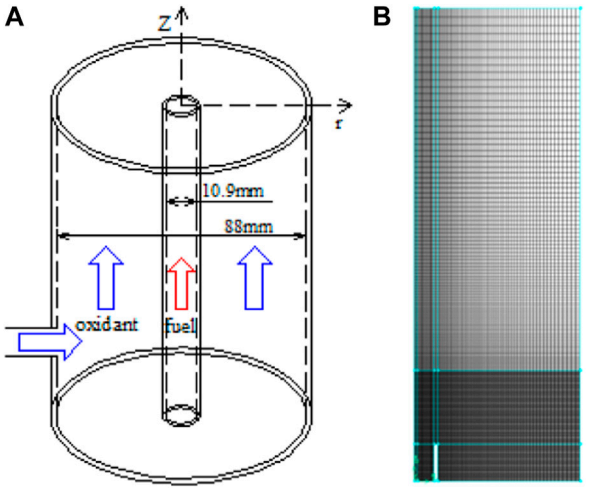


FIGURE 1
Schematic diagram of burner model **(A)** and grid division of the computational domain **(B)**.

## 2 Numerical simulation

### 2.1 Establishment of model

The numerical calculation model adopts the Gülder burner, similar to the literature (Zhang et al., 2019; Li et al., 2020; Liang et al., 2022). The inner diameter of the fuel tube of the burner is 10.9 mm, the wall thickness is 0.95 mm, and the inner diameter of the oxidant tube is 88 mm. The simplified model is shown in Figure 1A. The two-dimensional axisymmetric computational domain is adopted to reduce the amount of calculation, and finer grids are set in the primary reaction zone and the burner outlet. The numerical calculation domain is 11.8 cm ($z$) × 4.5 cm ($r$), which is divided into 194 ($z$) × 88 ($r$) control volumes. Figure 1B shows the calculation domain grid division. In the axial direction, the grid within 20 mm is divided into fine grids with a spacing of 0.2 mm. Then, the grid is set to change from dense to sparse with an expansion factor of 1.0205, a total of 94 nodes. In the radial direction, a fine grid with a spacing of 0.2 mm is adopted within 0.8 mm, 19 nodes are equally spaced within 0.8 mm–5.45 mm, four nodes are equally spaced within 5.45–6.45 mm, and then the grid is set to change from dense to sparse, with an expansion factor of 1.025, a total of 61 nodes. Considering the influence of fuel preheating, the calculation domain is extended 10 mm below the fuel nozzle of the burner., In addition, the computational domain includes the fuel nozzle to obtain a more reasonable nozzle fuel velocity distribution (Charest et al., 2011; Eaves et al., 2013).

## 2.2 Numerical solution method setting

The combustion model in this study is the laminar finite rate model, and the reaction rate is determined according to the Arrhenius formula. San Diego mechanism (Chemical-Kinetic Mechanisms for Combustion Applications, 2024) is selected as the chemical kinetic mechanism, and the reactions and components related to $NO_x$ formation are removed. The modified mechanism includes 175 steps of elementary reactions and 40 components. The numerical calculation solver is based on pressure coupling, and the numerical algorithm adopts Coupled to deal with the coupling of pressure and velocity. The Discrete coordinate (DO) radiation model is selected to calculate the radiation heat transfer, and the calculation equation is shown in Eq. 1. The weighted sum of the grey gas model (WSGG) is used to calculate the radiation characteristics of gas medium and soot.

$$\nabla \cdot (I_\lambda(\vec{r},\vec{s})\vec{s}) + (a_\lambda + \sigma_\lambda) I_\lambda(\vec{r},\vec{s}) = a_\lambda n^2 \mathrm{I}_{b\lambda} + \frac{\sigma_s}{4\pi}\int_0^{4\pi} \mathrm{I}_\lambda(\vec{r},\vec{s})\Phi\left(\vec{s},\overrightarrow{s'}\right)\mathrm{d}\Omega' \tag{1}$$

Where $\lambda$ is the radiation wavelength, $I$ is the radiation intensity, $\vec{r}$ is the position vector, $\vec{s}$ is the direction vector, $\overrightarrow{s'}$ is the scattering direction, $\Phi$ is scattering phase function, $n$ is the refractive coefficient, $\sigma_s$ is the scattering coefficient, $a_\lambda$ is the spectral absorption coefficient, $I_{b\lambda}$ is the black-body radiation intensity determined by PLANCK's law, $\Omega'$ is the solid space angle.

Moss Brookes model is adopted for the soot model (Brookes and Moss, 1999), and acetylene is selected for the soot precursor and surface growth. Lee model is selected for the oxidation model, and OH is the primary oxidant. The following Eq. 2 gives the instantaneous generation rate of soot particles:

$$\frac{dN}{dt} = \mathrm{a}N_A\left(\frac{X_{C_2H_2}P}{RT}\right)^l e^{-21100/T} - \left(\frac{24RT}{\rho_{Soot}N_A}\right)^{1/2} d_P^{1/2} N^2 \tag{2}$$

where $N$ is the soot particle number density ($m^{-3}$), a and $l$ are model constant, $N_A$ is the Avogadro number, $X$ is the mole fraction, $P$ is the pressure, Pa, $R$ is the gas constant, $T$ is the temperature, K, $d_P$ is the diameter of soot particles, $\rho_{Soot}$ is the mass density of soot, $t$ is time. The source term for the soot mass concentration is modeled by Eq. 3, including the soot mass produced by particle nucleation, the soot mass produced by the surface growth process, and the soot mass consumption by oxidation:

$$\begin{aligned}\frac{dM}{dt} = {} & M_P a\left(\frac{X_{C_2H_2}P}{RT}\right)^l e^{-12100/T} \\ & + b\left(\frac{X_{C_2H_2}P}{RT}\right)^m e^{-12100/T}\cdot\left[(\pi N)^{1/3}\left(\frac{6M}{\rho_{Soot}}\right)^{2/3}\right] \\ & -4.2325\frac{X_{OH}P}{RT}\sqrt{T}(\pi N)^{1/3}\left(\frac{6M}{\rho_{Soot}}\right)\end{aligned} \tag{3}$$

where $M$ is the soot mass density, kg/$m^3$, $M_P$ is the mass of primary soot particles, $b$, $m$, $n$ are additional model constants, $\rho_{Soot}$ is the mass density of soot, $t$ is time.

## 2.3 Boundary conditions and calculation conditions

This study selects the fuel and oxidant inlets as velocity inlets. The ethylene flow rate is 3.465 cm/s, the oxidant flow rate is 11.2 cm/s, and the temperature is 300 K. The lateral boundary is set as the isothermal wall of 300 K. The upper boundary is selected as the pressure outlet and allows the backflow of the outlet boundary. The nozzle wall temperature is set to 400 K for the heat transfer from the flame to the nozzle wall.

The eight groups of calculation conditions of adding $H_2$ and CO to ethylene/air diffusion flame are shown in Table 1. When adding $H_2$ or CO to the fuel, keep the ethylene flow rate constant at 194 mL/min. The total fuel flow rate increases with the increase of the blending ratio of $H_2$ and CO, and the oxidant flow rate (composed of 79% $N_2$, 21% $O_2$) is 40 L/min. The blending ratio φ is given by Eq. 4:

$$\phi = \frac{Q_i}{Q_i Q_{C_2H_4}} \tag{4}$$

Where, $Q_i$ is the flow rate of the gas blended in ethylene (mL/min), $Q_{C_2H_4}$ is the flow rate of ethylene (mL/min). 30% $FH_2$ and 30% FCO are added to the fuel to separate the chemical effect of $H_2$, and CO. $FH_2$ and FCO are chemically inert, do not participate in all relevant chemical reactions, and have the same thermochemistry and transport data as actual $H_2$ and CO.

# 3 Model rationality verification

The radial distribution of the temperature and soot volume fraction at the flame height of 30 mm is compared with the experimental data in the literature (Snelling et al., 2002) to verify the rationality of the model. The numerical simulation condition setting of case 1 is the same as that of the experimental literature condition. As shown in Figure 2, although the predicted soot volume fraction in the flame centerline region in Figure 2B is lower than the experimentally measured value, the variation trend of the two is consistent, and both increase first and then decrease with the increase of the flame radius. The main reason for the difference in the area near the central axis is that the current soot model cannot reasonably predict the soot surface growth caused by polycyclic aromatic hydrocarbon condensation (Frenklach et al., 2000). As a result, this lowers the soot volume fraction of the numerical simulation in the central axis area. This study only explores the effect of blending on the peak volume fraction of soot. It can be seen from the figure that the numerical simulation results in this paper are consistent with the variation trends of temperature and soot volume fraction in the literature, and the peak position of soot volume fraction in the flame is basically consistent. The maximum temperature error is about 1.81%, and the peak error of the soot volume fraction is about 0.03%. Thus, the rationality of this model can be guaranteed.

# 4 Results and discussion

## 4.1 Temperature

Temperature distribution is an important indicator for describing the combustion characteristics of flames. Figure 3A shows the two-dimensional distribution and peaks of the flame temperature in case 1, case 2, case 3, case 4, case 5, case 6, and case 7. In the pure ethylene flame, the peak temperature is 2146.3 K, which

TABLE 1 Calculation conditions.

| Case | Blending ratio | | Q ($C_2H_4$)/ ($mL·min^{-1}$) | Q ($H_2$)/ ($mL·min^{-1}$) | Q ($FH_2$)/ ($mL·min^{-1}$) | Q (CO)/ ($mL·min^{-1}$) | Q (FCO)/ ($mL·min^{-1}$) |
|---|---|---|---|---|---|---|---|
| | φ($H_2$/ $FH_2$) | φ(CO/ FCO) | | | | | |
| 1 | 0 | 0 | 194 | 0 | 0 | 0 | 0 |
| 2 | 15% | 0 | 194 | 34.24 | 0 | 0 | 0 |
| 3 | 30% | 0 | 194 | 83.14 | 0 | 0 | 0 |
| 4 | 30% | 0 | 194 | 0 | 83.14 | 0 | 0 |
| 5 | 0 | 15% | 194 | 0 | 0 | 34.24 | 0 |
| 6 | 0 | 30% | 194 | 0 | 0 | 83.14 | 0 |
| 7 | 0 | 30% | 194 | 0 | 0 | 0 | 83.14 |
| 8 | 10% | 20% | 194 | 27.71 | 0 | 55.43 | 0 |
| 9 | 15% | 15% | 194 | 41.57 | 0 | 41.57 | 0 |
| 10 | 20% | 10% | 194 | 55.43 | 0 | 27.71 | 0 |
| 11 | 20% | 20% | 194 | 64.67 | 0 | 64.67 | 0 |

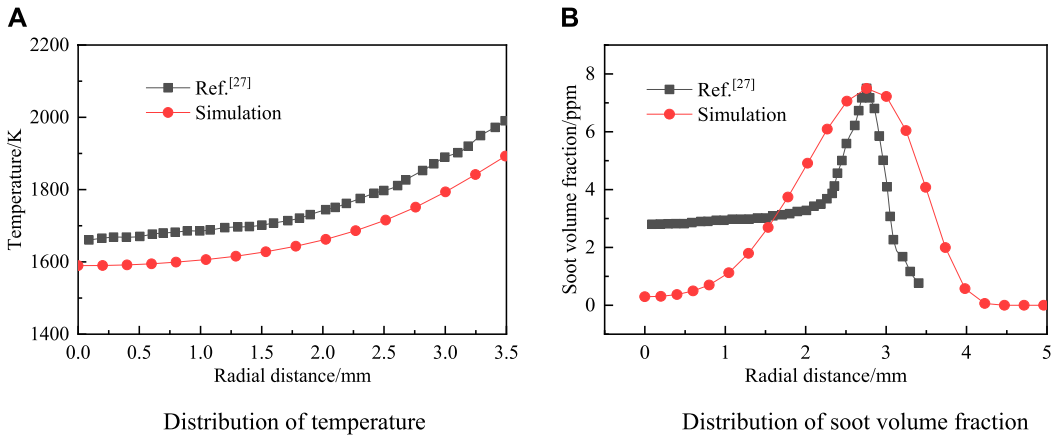


FIGURE 2
Radial distribution of temperature **(A)** and soot volume fraction **(B)** at 30 mm cross section of flame.

appears in the lower annular region of the flame about 1.12 cm above the burner outlet and about 0.62 cm radially from the central axis. When ethylene is blended with 30%$H_2$, the peak temperature increases by about 26 K; when 30%CO is blended, the peak temperature increases by about 7 K. Both $H_2$ and CO blending increase the peak temperature slightly and appear at a higher axial height. When blending 30%$FH_2$ and 30%FCO, the peak temperature is about 46 K and 23 K lower than pure ethylene flame. The reason is that $H_2$ and CO participate in the chemical reaction of combustion and release heat to increase the flame temperature. However, the $FH_2$ and FCO are inert; only the dilution effect reduces the mole concentration of ethylene in the fuel stream, resulting in a reduction in the intensity of the combustion reaction and, thus, lower flame temperature. The blending of 30%$H_2$ and 30%CO only increased the peak temperature by 1.2% and 0.3%, respectively, and had no significant effect on the flame temperature.

Figure 3B shows the temperature distribution of the flame center axis in case 1, case 2, case 3, case 5, and case 6. As shown in the figure, downstream region of the flame (below $z = 5$ cm), the blending of $H_2$ and CO does not affect the flame temperature near the centerline. The flame temperature gradually increased with a high $H_2$ and CO blending ratio in the centerline region near the flame tip. This is because blending $H_2$ and CO reduces the soot load upstream of the flame and leads to radiant heat loss, resulting in a slight increase in temperature.

## 4.2 Soot

### 4.2.1 Soot formation

The mechanism of soot generation is related to dilution effect, thermal effect, and chemical effect. Figure 4A shows the two-

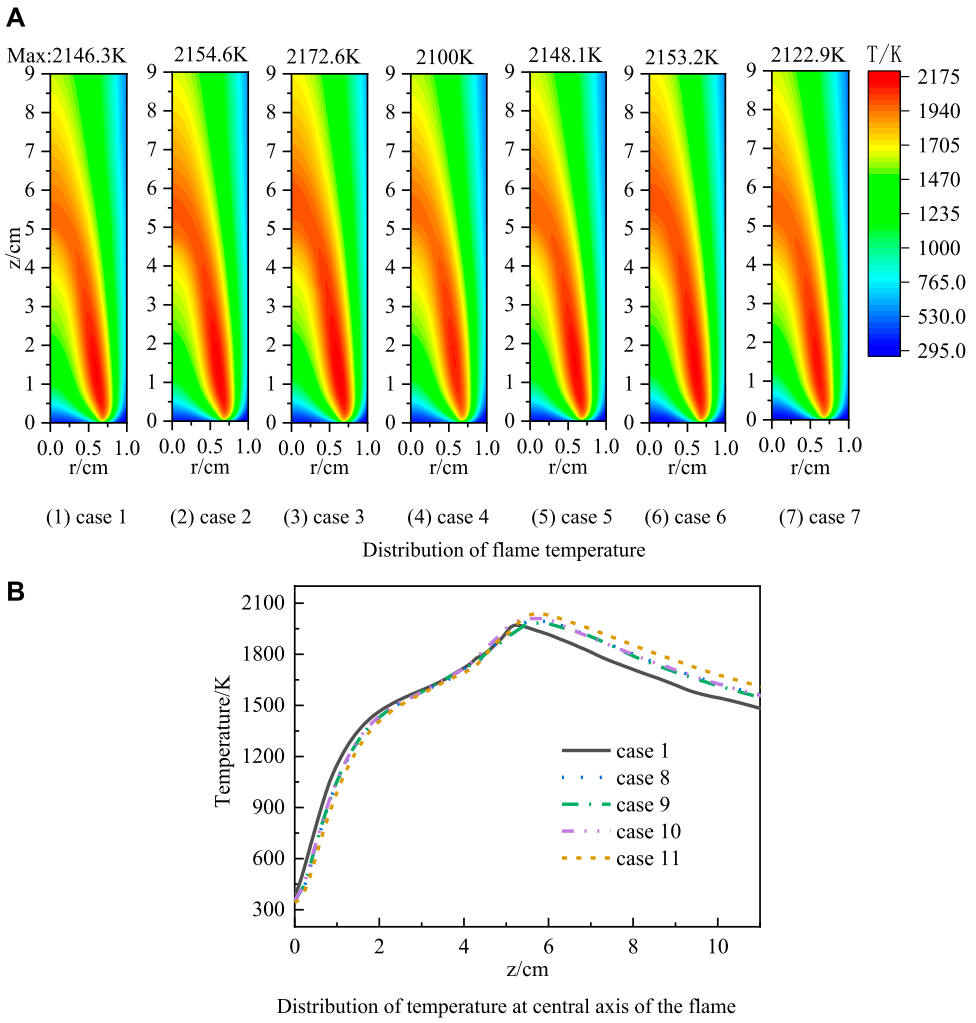


FIGURE 3
Distribution of flame temperature **(A)** and temperature central axis of the flame **(B)**.

dimensional distribution of the soot volume fraction and the peak soot volume fraction in the flame for Case 1, Case 3, Case 4, Case 6, Case 7, and Case 8. Pure ethylene peak soot volume fraction is 7.635 ppm, in the annular region of $z = 2.61$ cm and $r = 0.3$ cm. The peak soot volume fraction decreased by 0.977 ppm after blending 30% $H_2$ in ethylene, and the peak soot volume fraction decreased by 0.726 ppm after blending 30% CO. When 15% $H_2$ and 15% CO are blended simultaneously, the peak soot volume fraction is 6.908 ppm, between the peak soot volume fraction when 30% $H_2$ and 30% CO are blended. The peak soot volume fraction still appears at the two wings of the flame. Adding $H_2$ and CO can slightly increase the soot appearance position, indicating that $H_2$ or CO can inhibit the soot nucleation. Comparing the soot distribution of case 3 and 4, and case 6 and 7, it can be seen that the soot volume fraction is further reduced after blending 30% $FH_2$ and 30% FCO, and the chemical effect of $H_2$ and CO promotes the soot formation in the ethylene flame. Blending $H_2$ and CO both inhibits the soot formation, and the inhibition effect of $H_2$ is more significant under the same blending ratio because the chemical effect of CO has a substantially better promoting effect on soot formation. The conclusion drawn from 4.1 is that the mixing of $H_2$ and CO does not have a significant impact on temperature, so the thermal effect is not the main reason for the change in soot generation. The dilution effect is mainly due to the mixing of $H_2$ and CO, which reduces the carbon content per unit mass of fuel gas mixture and thus reduces the amount of soot generated. The inhibition of blending $H_2$/CO on the soot formation is mainly due to the dilution effect.

Figure 4B shows the radial distribution of the soot volume fraction of case 1, case 2, case 3, case 5, and case 6 at the flame height of 3 cm. It can be seen from the figure that as the $H_2$/CO blending ratio increases, the soot volume fraction gradually decreases, and the soot distribution region moves away from the center axis and becomes narrower. Under the same blending ratio, adding $H_2$ decreases the soot volume fraction, and the inhibition effect on soot is more significant.

Figure 5A shows the distribution of soot volume fraction along the flame axial of pure ethylene flame and ethylene blended with 30% $H_2$, 30% $FH_2$, 30% CO, and 30% FCO, respectively. The following Equation obtains the integral of the soot volume fraction of the flame cross-section:

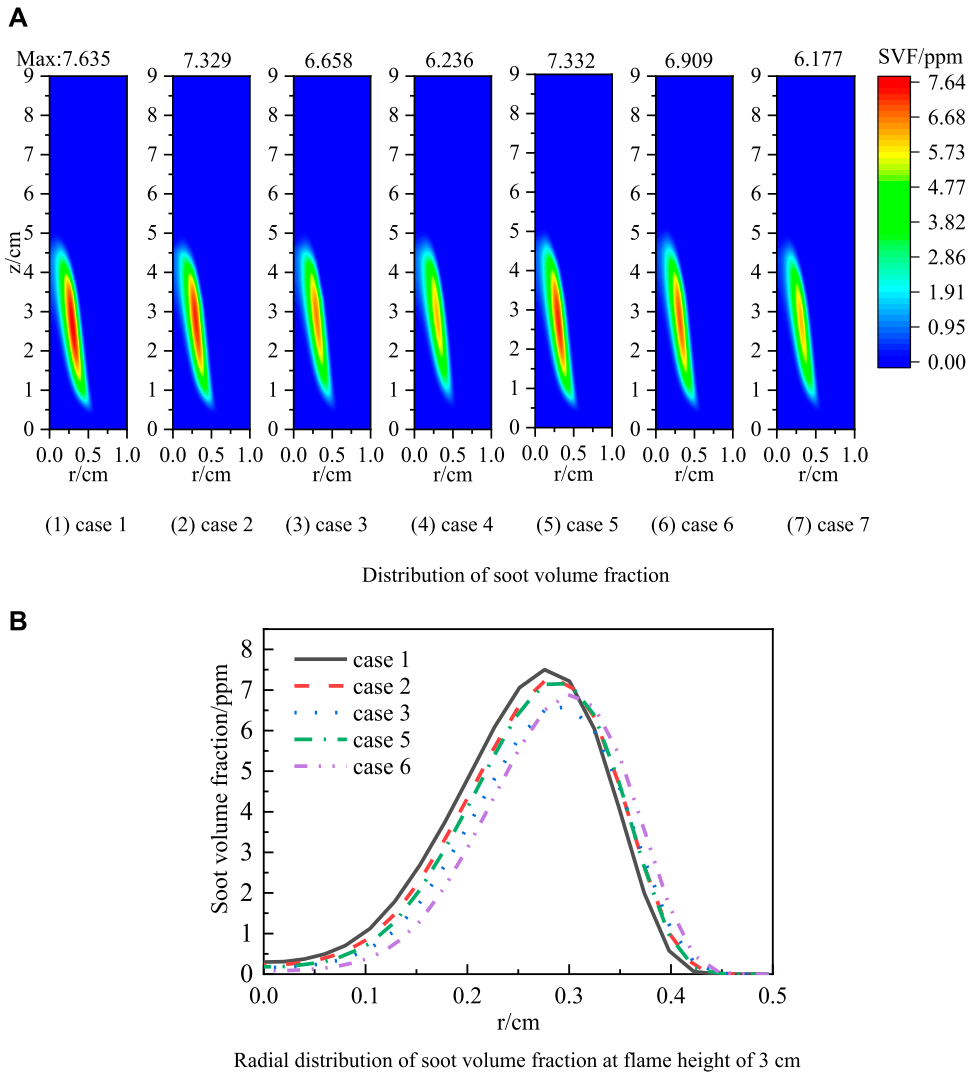


FIGURE 4
Distribution of soot volume fraction **(A)** and Radial distribution of those at flame height of 3 cm **(B)**.

$$F_v(z) = \int 2\pi r f_v(r,z) dr \quad (5)$$

where $f_v(r,z)$ is the local soot volume fraction. The results again show that blending $H_2$ or CO in ethylene will reduce the soot volume fraction, and the peak of the soot volume fraction appears at the higher flame height. It can be seen from the figure that blending $FH_2$ or FCO reduces the soot volume fraction by a greater extent than blending $H_2$ or CO, indicating that the chemical effect of $H_2$ and CO promotes the soot formation. It can be seen from Figure 5B that under the condition of adding $H_2$ and CO with the same proportion, the peak soot volume fraction decreases with the increase of mixing proportion, and the radial distribution function area of the soot narrows and moves to the right. Adding $H_2$/CO inhibits the formation of soot. With the same proportion of $H_2$ and CO added, the soot volume fraction gradually decreases as the total $H_2$/CO blending ratio increases. When the total $H_2$/CO blending ratio is the same, the larger the $H_2$ blending ratio, the more significant the decrease in the volume fraction of soot. $H_2$ has a more significant inhibitory effect on soot under the same mixing ratio.

### 4.2.2 The chemical effect of $H_2$

In the diffusion flame, soot surface growth is the essential process leading to the increase of soot volume fraction in the flame (Guo et al., 2006; Kalbhor and Oijen, 2020). Temperature, $C_2H_2$, and H concentration are the main factors affecting soot surface growth. Figure 6A shows the radial temperature distribution under different axial heights. It can be seen from the figure that adding $H_2$ improves the flame temperature on the whole. At $z$ = 1 cm, the flame temperature of pure ethylene is higher than that of the ethylene blended with 30% $FH_2$. The two become close with the increase of the flame height, which indicates that the dilution effect of blending $FH_2$ at the lower flame height reduces the flame temperature. While at the higher flame height, the influence of thermal radiation loss dominated by soot is increasingly essential. Blending 30% $FH_2$ reduces the radiation

10.3389/fenrg.2024.1363363

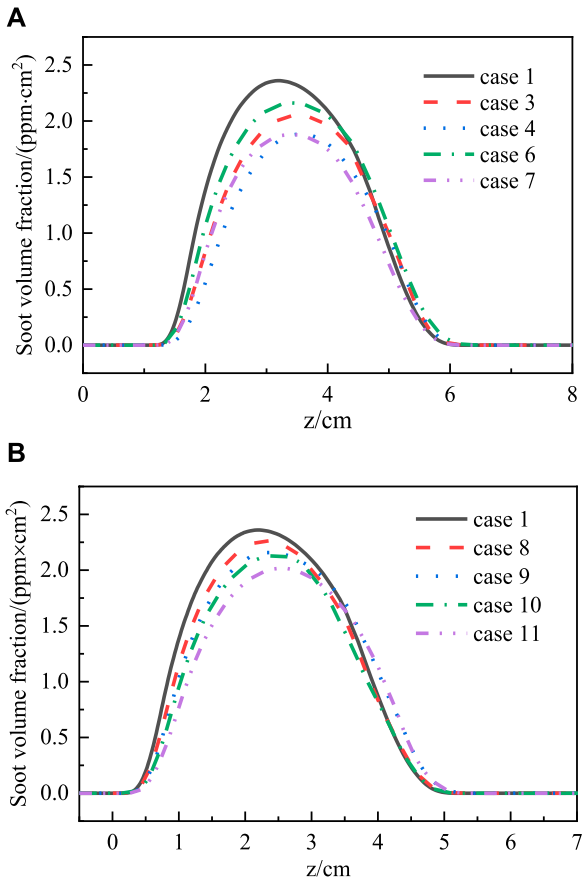


FIGURE 5
Distributions of flame cross-sectional area integrated soot volume fraction along the flame height **(A,B)**.

heat loss due to suppressing soot load. Thus, at $z$ = 3.5 cm, the temperature of blending 30%$FH_2$ is slightly higher than that of pure ethylene. Comparing the temperature curves of blending 30% $H_2$ and 30% $FH_2$ indicates that the chemical effect of hydrogen increases the flame temperature slightly on the whole.

Figure 6B shows the radial distribution of the $C_2H_2$ mole fraction at flame heights of 1 cm, 2 cm, and 3.5 cm. The results show that the $C_2H_2$ mole fraction decreases after blending $H_2$, while the chemical effect of $H_2$ increases the $C_2H_2$ mole fraction. This is because the peak flame temperature blended with 30% $H_2$ is higher than that of the blended 30%$FH_2$. As a result, this leads to the accelerated pyrolysis of ethylene, thereby promoting the formation of $C_2H_2$.

The H radical controls the formation rate of active sites in the $C_2H_2$ addition reaction (Guo et al., 2009). Figure 6C shows the radial distribution of the H mole fraction at flame heights of 1 cm, 2 cm, and 3.5 cm. It can be seen from Figure 6C that the chemical effect of $H_2$ increases the H mole fraction. By analyzing the reactions involving H radicals, the following are the reactions that have the primary effect on H radicals when $H_2$ is blended:

$$H_2 + O = OH + H \quad (R2)$$
$$H_2 + OH = H_2O + H \quad (R3)$$

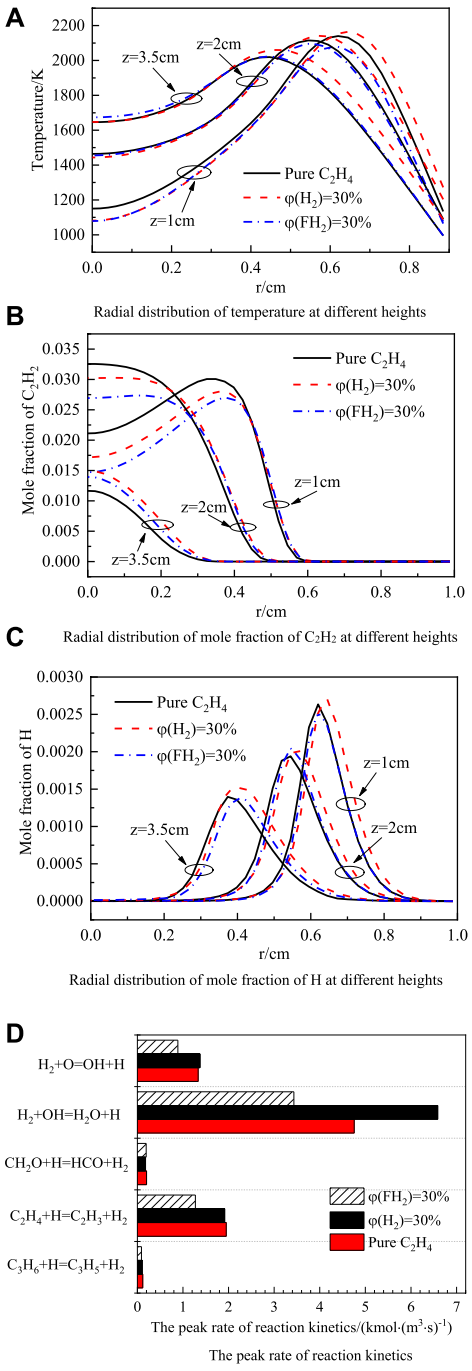


FIGURE 6
Radial distribution of temperature **(A)**, mole fraction of $C_2H_2$ **(B)**, mole fraction of H **(C)** at different heights and the peak rate of reaction kinetics **(D)**.

$$CH_2O + H = HCO + H_2 \quad (R32)$$
$$C_2H_4 + H = C_2H_3 + H_2 \quad (R84)$$
$$C_3H_6 + H = C_3H_5 + H_2 \quad (R152)$$

Figure 6D shows the peak rate changes of these reactions. It can be seen from the figure that H2+OH = H2O + H, H2+O=OH + H are the main generation reactions of H, and C2H4+H=C2H3+H2 is the main consumption reaction of H. The elementary reaction

10.3389/fenrg.2024.1363363

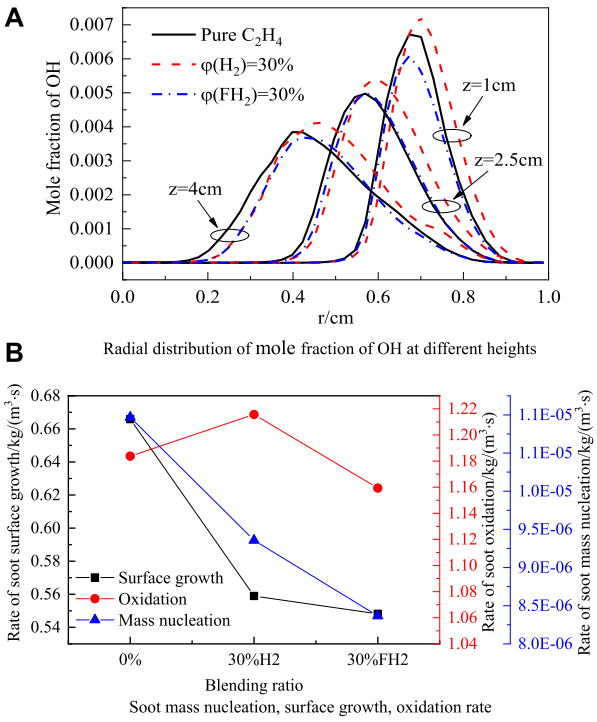


FIGURE 7
Radial distribution of mole fraction of OH at different heights **(A)** and Soot mass nucleation, surface growth, oxidation rate **(B)**.

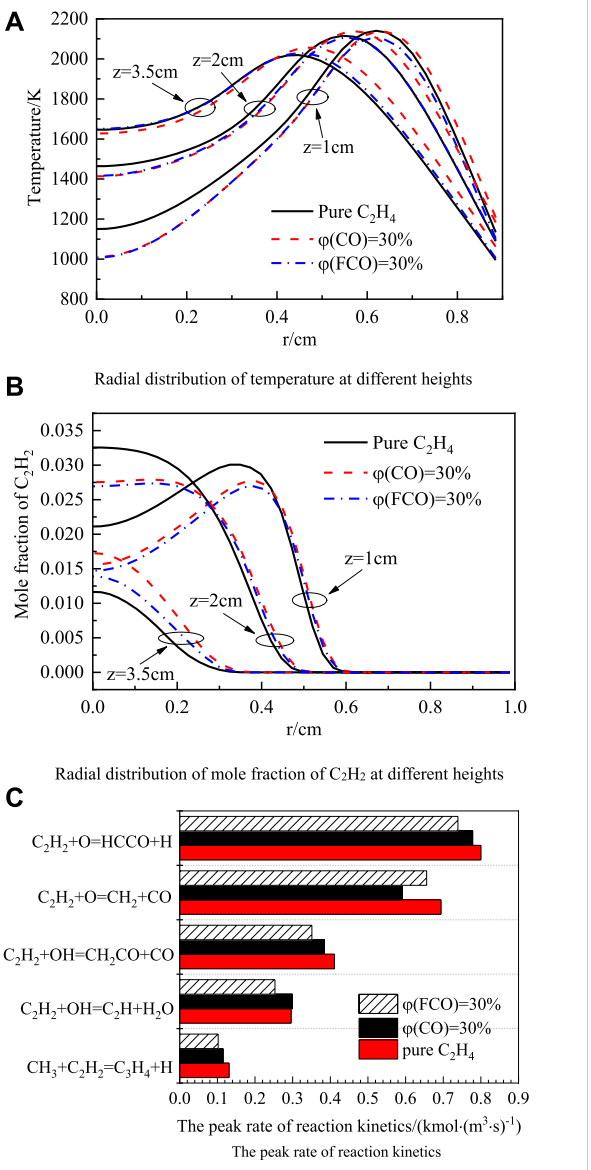


FIGURE 8
Radial distribution of temperature **(A)**, mole fraction of $C_2H_2$ at different heights **(B)** and the peak rate of reaction kinetics **(C)**.

$H_2$+OH = $H_2O$ + H is most sensitive to the chemical effect of $H_2$. As the mole fraction of $H_2$ increases, the above elementary reaction proceeds forward to generate more H, while as the mole fraction of $FH_2$ increases, the above elementary reaction rate is lower than the baseline operating condition. In the elementary reaction $H_2$+O=OH + H, the chemical effect of $H_2$ is also significant. Under the $H_2$ chemical effect, the two elementary reactions together increase the molar fraction of H, which is greater than the consumption of H radicals, thereby increasing the concentration of H radicals.

OH plays an essential role in the oxidation process of soot, and Figure 7A shows the radial distribution of OH mole fractions at $z$ = 1 cm, $z$ = 2.5 cm, and $z$ = 4 cm. It can be seen from the figure that the overall OH mole fraction distribution moves away from the flame centerline after blending $H_2$. This is because, under the chemical effect of $H_2$, the flame height increases, and the peak OH concentration region moves away from the flame centerline. Overall, the $H_2$ blend increases the mole fraction of OH because the $H_2$ chemical effect accelerates the forward reaction rate of $H_2$ + O = OH + H and increases the OH concentration. However, as shown in Figure 4A, the soot is mainly distributed at the two wings of the flame closer to the flame centerline rather than the main distribution area of OH radicals. It can be seen from Figure 7A that the difference in the OH mole fraction of blending 30% $H_2$ and 30% $FH_2$ in the area near the flame centerline is not apparent.

Figure 7B shows rates of soot mass nucleation, surface growth, and oxidation of pure ethylene blended with 30% $H_2$ and 30% $FH_2$. It can be seen from the figure that the mass nucleation and surface growth rates of soot are significantly reduced after blending $H_2$. As a result, the surface growth and mass nucleation rates of soot are further reduced by blending $FH_2$, indicating that the chemical effect of $H_2$ inhibits soot nucleation and surface growth. The soot oxidation rate is slightly increased by blending $H_2$, while the oxidation rate is slightly decreased by blending $FH_2$. The chemical effect of $H_2$ promoted the oxidation of soot. Under the competition of the formation and consumption rate of soot, it finally manifests as the chemical effect of $H_2$ promotes the soot formation.

### 4.2.3 The chemical effect of CO

Figure 8A shows the radial temperature distribution at 1 cm, 2 cm, and 3.5 cm in the axial direction. It can be seen from the figure that the temperature in the blended CO flame is higher than that in the blended FCO flame. The reason is that CO actively participates in the chemical reaction and releases heat, while FCO does not. Thus, the chemical effect of blending CO increases the flame

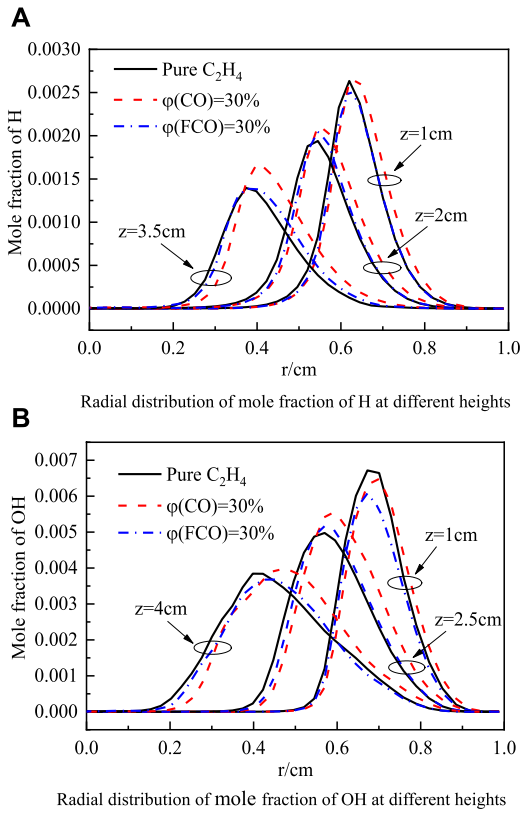


FIGURE 9
Radial distribution of mole fraction of H **(A)** and OH **(B)** at different heights.

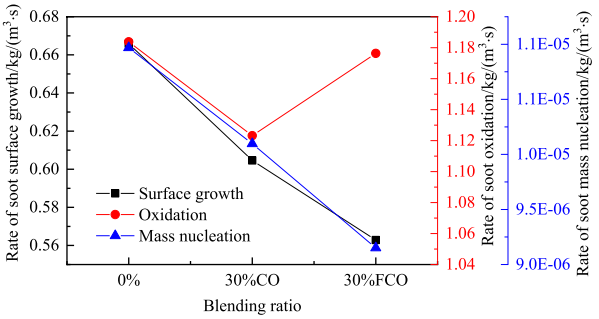


FIGURE 10
Soot mass nucleation, surface growth, oxidation rate.

temperature. A higher temperature is beneficial to increase the addition rate of $C_2H_2$ and promote the surface growth of soot.

Figure 8B shows the radial distribution of the $C_2H_2$ mole fraction at different axial heights. The results show that the blending CO reduces the $C_2H_2$ mole fraction at the lower part of the flame, and the $C_2H_2$ mole fraction in the blending CO flame is slightly higher than that in the blending FCO flame at different heights. Figure 8C shows the $C_2H_2$ consumption reaction rate change. It can be seen from the figure that the reaction $C_2H_2 + O = CH_2 + CO$ is one of the most critical consumption reactions of $C_2H_2$, which is consistent with the literature (Dai et al., 2021). $C_2H_2$+O=$CH_2$+CO is most sensitive to the chemical effects of CO. Compared with the addition of FCO, the forward reaction rate of this reaction is reduced after adding CO, and the $C_2H_2$ consumption rate is slowed down, resulting in higher $C_2H_2$ concentration. But under the CO chemical effect, the forward reaction rate of other elementary reactions accelerates, and the consumption rate of C2H2 increases. SO as seen in Figure 8B, the chemical effect of CO increases the $C_2H_2$ mole fraction slightly, but the difference is not significant.

The radial distribution of H radicals at different axial heights is shown in Figure 9A. Overall, the H mole fractions in the blending FCO and pure ethylene flame are not significantly different, while the H mole fraction in the blending CO flame is higher than that in the blending FCO flame. This is due to the increase in the forward reaction rate of the reaction CO + OH = H + $CO_2$ with the addition of CO, and the H radical concentration increases. This indicates that the chemical effect of CO increases the H mole fraction, and the higher H mole fraction enhances the formation rate of active centers in the blended CO flame and ultimately increases the surface growth rate.

OH is the predominant soot oxidant, and Figure 9B shows the OH radical mole fraction distribution at different axial heights. It can be seen from the figure that in the blending CO flame, the OH mole fraction in the near centerline region where soot exists (the soot distribution region shown in Figure 4) is lower than that in the blending FCO flame. It is also due to the reaction CO + OH = H + $CO_2$; when CO is added, the forward reaction rate increases, speeding up the consumption of OH. Lower OH concentration is beneficial to slow down the soot oxidation rate in the flame and increase the rate of net soot formation. It indicates that the chemical effect of CO inhibits soot oxidation.

Figure 10 shows the soot mass nucleation rate, surface growth rate, and oxidation rate of the pure ethylene blended with 30% CO and 30% FCO. The results show that the soot mass nucleation and surface growth rates are reduced by adding CO. Also, the soot mass nucleation and surface growth rates are further decreased after adding FCO, indicating that the chemical effect of CO inhibits soot nucleation and surface growth. Adding both CO and FCO can reduce the oxidation rate to some extent. Compared with blending CO, the oxidation rate of blending FCO is higher. The chemical effect of CO inhibited soot oxidation.

## 5 Conclusion

In this paper, the effect of $H_2$/CO blending on soot formation in laminar ethylene/air diffusion flames is studied by numerical simulation. The non-reactive virtual substances $FH_2$ and FCO are set in the numerical calculation to separate the chemical effects of $H_2$ and CO. The distribution of temperature, soot, and important intermediate components is analyzed, and the following main conclusions are obtained:

(1) In the laminar flow ethylene/air diffusion flame, the flame temperature gradually increases with the increase of the

$H_2$/CO blending ratio, but the change is insignificant. Blending 30% $H_2$ increased the temperature by 1.2%, and blending 30% CO increased the temperature by 0.3%. The thermal effect of $H_2$/CO is not the main factor affecting soot formation.

(2) With the increase in the $H_2$/CO blending ratio, the soot volume fraction of the laminar diffusion flame decreases monotonically. At the same blending ratio, the inhibitory effect of $H_2$ on soot is more effective due to the more substantial promotion effect of the chemical effect of CO on soot. The soot volume fraction decreases after the simultaneous blending of $H_2$ and CO, and the peak soot volume fraction is between that of the blending of $H_2$ and CO. The inhibition of soot formation by blending $H_2$ or CO is mainly the dilution effect.

(3) The chemical effect of blending $H_2$ increases the flame temperature, the mole fraction of $C_2H_2$ and H, and the soot nucleation, surface growth, and oxidation rates. It finally manifests as the chemical effect of $H_2$ promotes the soot formation under the competition of the formation and consumption rate of soot.

(4) The chemical effect of CO increases the flame temperature, increases the H mole fraction, and decreases the OH mole fraction, thus increasing the soot surface growth rate and slowing down the soot oxidation rate. Higher nucleation and surface growth rates and lower oxidation rates jointly promote soot formation.

## Data availability statement

The original contributions presented in the study are included in the article/Supplementary material, further inquiries can be directed to the corresponding author.

## Author contributions

YZ: Funding acquisition, Supervision, Writing -review and editing. YiX: Methodology, Validation, Writing -review and editing. ZX: Writing -Original draft and Writing -review and editing. FZ: Software, Validation, Writing -review and editing. YuX: Investigation, Writing -original draft. QC: Writing -Original draft and Writing -review and editing. ST: Data curation, Writing -review and editing.

## Funding

The author(s) declare that financial support was received for the research, authorship, and/or publication of this article. The authors acknowledge the financial support of the National Natural Science Foundation of China (Nos 52274060 and 51974033), the Yangtze Youth Talents Fund (No. 2015cqt01) and Leading talents of Yangtze talent plan.

## Conflict of interest

The authors declare that the research was conducted in the absence of any commercial or financial relationships that could be construed as a potential conflict of interest.

## Publisher's note



## References

Brookes, S. J., and Moss, J. B. (1999). Predictions of soot and thermal radiation properties in confined turbulent jet diffusion flames. *Combust. Flame* 116 (4), 486–503. doi:10.1016/s0010-2180(98)00056-x

Charest, M., Groth, C., and Gülder, O. L. (2011). Effects of gravity and pressure on laminar coflow methane-air diffusion flames at pressures from 1 to 60 atmospheres. *Combust. Flame* 158 (5), 860–875. doi:10.1016/j.combustflame.2011.01.019

Chemical-Kinetic Mechanisms for Combustion Applications (2024). *San Diego mechanism web page, mechanical and aerospace engineering (combustion research)*. San Diego: University of California. Available at: http://combustion.ucsd.edu.

Cocean, I., Cocean, A., Pohoata, V., and Gurlui, S. (2020). City water pollution by soot-surface-active agents revealed by FTIR spectroscopy. *Appl. Surf. Sci.* 499, 142487. doi:10.1016/j.apsusc.2019.04.179

Dai, W., Yan, F., Xu, L., Zhou, M., and Wang, Y. (2020). Effects of carbon monoxide addition on the sooting characteristics of ethylene and propane counterflow diffusion flames. *Fuel* 271, 117674. doi:10.1016/j.fuel.2020.117674

Dai, W., Yan, F. W., and Wang, Y. (2021). Effect of carbon monoxide addition on sooting characteristics of methane flames. *J. Hefei Univ. Technol. Nat. Sci.* 44 (8), 1013–1020. doi:10.3969/j.issn.1003-5060.2021.08.002

Eaves, N. A., Thomson, M. J., and Dworkin, S. B. (2013). The effect of conjugate heat transfer on soot formation modeling at elevated pressures. *Combust. Sci. Technol.* 185 (10-12), 1799–1819. doi:10.1080/00102202.2013.839554

Frenklach, B. M., Bockhorn, H., and Frenklach, M. (2000). Kinetic modeling of soot formation with detailed chemistry and physics: laminar premixed flames of C2 hydrocarbons. *Combust. Flame* 121 (1-2), 122–136. doi:10.1016/s0010-2180(99)00135-2

Guo, H., Liu, F., Smallwood, G. J., and Gülder, Ö. L. (2006). Numerical study on the influence of hydrogen addition on soot formation in a laminar ethylene–air diffusion flame. *Combust. Flame* 145 (1/2), 324–338. doi:10.1016/j.combustflame.2005.10.016

Guo, H., Thomson, K. A., and Mallwood, G. J. (2009). On the effect of carbon monoxide addition on soot formation in a laminar ethylene/air coflow diffusion flame. *Combust. Flame* 156 (6), 1135–1142. doi:10.1016/j.combustflame.2009.01.006

Jiang, Y., and Qiu, R. (2010). Numerical analysis of the effect of carbon monoxide addition on soot formation in an acetylene/air premixed flame. *ACTA PHYSICO-CHIMICA SIN.* 26 (8), 128–132. doi:10.3866/PKU.WHXB20100823

Kalbhor, A., and Oijen, J. (2020). Effects of hydrogen enrichment and water vapour dilution on soot formation in laminar ethylene counterflow flames. *Int. J. Hydrogen Energy* 45 (43), 23653–23673. doi:10.1016/j.ijhydene.2020.06.183

Krishnamoorthi, M., Sreedhara, S., and Duvvuri, P. P. (2020). Experimental, numerical and exergy analyses of a dual fuel combustion engine fuelled with syngas and biodiesel/diesel blends. *Appl. Energy* 263, 114643. doi:10.1016/j.apenergy.2020.114643

Lapalme, D., Halter, F., Mounaim-Rousselle, C., and Seers, P. (2018). Characterization of thermos diffusive and hydrodynamic mechanisms on the cellular instability of syngas fuel blended with $CH_4$ or $CO_2$. *Combust. Flame* 193 (JUL), 481–490. doi:10.1016/j.combustflame.2018.03.028

Li, H., Pang, B., Zhu, F. H., Sun, X. L., Xu, J. X., and Wang, S. (2022). Comparative energy consumption structure and mode between China and major energy consuming countries under the background of carbon emission reduction. *Environ. Sci.*, 1–13. doi:10.13227/j.hjkx.202112065

Li, Z. C., Zhang, L. D., and Lou, C. (2020). *In-situ* measurement of soot volume fraction and temperature in axisymmetric soot-laden flames using TR-GSVD

algorithm. *IEEE Trans. Instrum. Meas.* 70 (99), 1–12. doi:10.1109/tim.2020.3010592

Liang, B. W., Wang, C. J., Zhang, Y. D., Bing, L., Fanjin, Z., Takyi, S. A., et al. (2022). Effect of $CO_2$/$H_2O$ addition on laminar diffusion flame structure and soot formation of oxygen-enriched ethylene. *J. Energy Inst.* 102, 160–175. doi:10.1016/j.joei.2022.03.007

Mahgoub, B., Suhaimi, H., Anwar, S. S., Mamat, R., Abdullah, A. A., and Hagos, F. Y. (2017). Combustion and performance of syngas dual fueling in a CI engine with blended biodiesel as pilot fuel. *Bioresources* 12 (3), 5617–5631. doi:10.15376/biores.12.3.5617-5631

Qiu, L., Hua, Y., Zhuang, Y., Wei, J., Qian, Y., and Cheng, X. (2020). Numerical investigation into the decoupling effects of hydrogen blending on flame structure and soot formation in a laminar ethylene diffusion flame. *Int. J. Hydrogen Energy* 45 (31), 15672–15682. doi:10.1016/j.ijhydene.2020.04.033

Sahu, R., Adak, P., and Elumalai, S. P. (2016). Characterization of hazardous solid waste (soot) accumulated in tailpipe of typical Indian share autos. *Curr. Sci.* 111 (3), 560–564. doi:10.18520/cs/v111/i3/560-564

Shiraiwa, M., Selzle, K., and Pöschla, U. (2012). Hazardous components and health effects of atmospheric aerosol particles: reactive oxygen species, soot, polycyclic aromatic compounds and allergenic proteins. *Free Radic. Res.* 46 (8), 927–939. doi:10.3109/10715762.2012.663084

Snelling, D. R., Thomson, K. A., Smallwood, G. J., Gulder, O. L., Weckman, E. J., and Fraser, R. A. (2002). Spectrally resolved measurement of flame radiation to determine soot temperature and concentration. *Aiaa J.* 40 (9), 1789–1795. doi:10.2514/3.15261

Sun, Z. W., Dally, B., Nathan, G., and Alwahabi, Z. (2017). Effects of hydrogen and nitrogen on soot volume fraction, primary particle diameter and temperature in laminar ethylene/air diffusion flames. *Combust. Flame* 175, 270–282. doi:10.1016/j.combustflame.2016.08.031

Wang, K., Zhang, Y. D., Wang, C. J., and Xin, Y. (2021a). Numerical simulation of combustion of $CH_4$ mixed $H_2$ and rationality analysis of premixed ratio. *Chin. J. Process Eng.* 21 (2), 240–250. doi:10.12034/j.issn.1009-606X.220058

Wang, Y., Gu, M. Y., Chao, L., Wu, J., Lin, Y., and Huang, X. (2021b). Different chemical effect of hydrogen addition on soot formation in laminar coflow methane and ethylene diffusion flames. *Int. J. Hydrogen Energy* 46 (29), 16063–16074. doi:10.1016/j.ijhydene.2021.02.014

Wang, Y., Liu, X., Gu, M., and An, X. (2018). Numerical simulation of the effects of hydrogen addition to fuel on the structure and soot formation of a laminar axisymmetric coflow $C_2H_4$/($O_2$-$CO_2$) diffusion flame. *Combust. Sci. Technol.* 191, 1743–1768. doi:10.1080/00102202.2018.1532413

Yen, M., Magi, V., and Abraham, J. (2019). Modeling the effects of hydrogen and nitrogen addition on soot formation in laminar ethylene jet diffusion flames. *Chem. Eng. Sci.* 196, 116–129. doi:10.1016/j.ces.2018.07.061

Zeng, S., Su, B., Zhang, M., Gao, Y., Liu, J., Luo, S., et al. (2021). Analysis and forecast of China's energy consumption structure. *Energy Policy* 159, 112630. doi:10.1016/j.enpol.2021.112630

Zhang, Y., Liu, F., Clavel, D., Smallwood, G. J., and Lou, C. (2019). Measurement of soot volume fraction and primary particle diameter in oxygen enriched ethylene diffusion flames using the laser-induced incandescence technique. *Energy* 177 (JUN.15), 421–432. doi:10.1016/j.energy.2019.04.062

Zhao, H., Stone, R., and Williams, B. (2014). Investigation of the soot formation in ethylene laminar diffusion flames when diluted with helium or supplemented by hydrogen. *Energy & fuels* 28 (3), 2144–2151. doi:10.1021/ef401970q